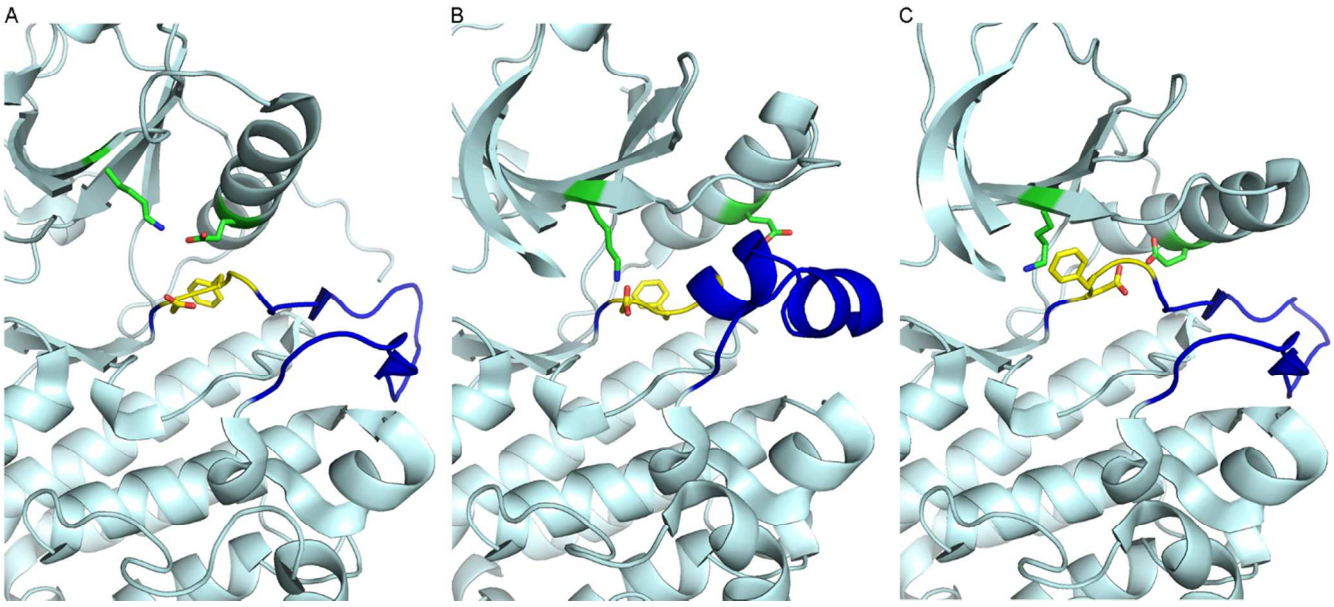

Figure S1. Three structures of EGFR kinase domain experimentally determined. A) DFG-in active conformation (PDB entry 2ITW). B) Src-like inactive conformation (PDB entry 3W32). C) DFG-out inactive conformation (PDB entry 4I20). The activation loop (A-loop) is colored blue; carbon atoms of the DFG motif are colored yellow; carbon atoms of Lys745 and Glu762 are colored green. The DFG-in active form adopts the DFG-in conformation; Lys745 and Glu762 form a salt bridge; the A-loop is in the extended state. The Src-like inactive form adopts the DFG-in conformation; Lys745 and Glu762 are separated; the A-loop is packed. The DFG-out form adopts the DFG-out conformation; Lys745 and Glu762 are apart from each other; the A-loop is extended.

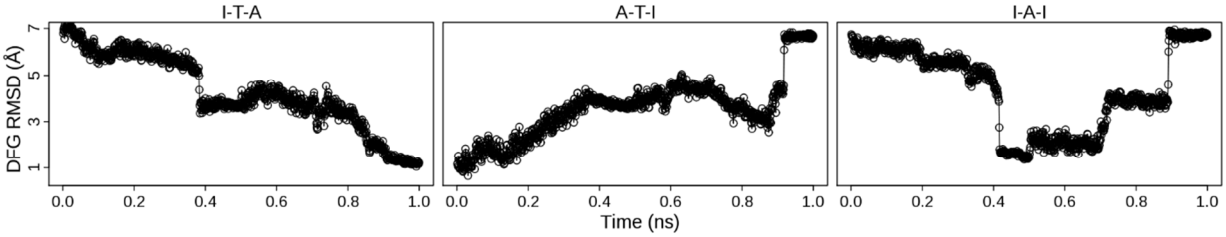

Figure S2. Time evolution of DFG RMSD in MTMD simulations. The crystal structure of 2ITW (form A) adopts the DFG-in conformation and is used as the reference structure. Sampled structures from MTMD trajectories are superposed onto the reference structure using backbone atoms to remove overall rotation and translation. Then heavy-atom RMSD values of DFG motif (residues 855 – 857) are calculated with respect to the reference structure.

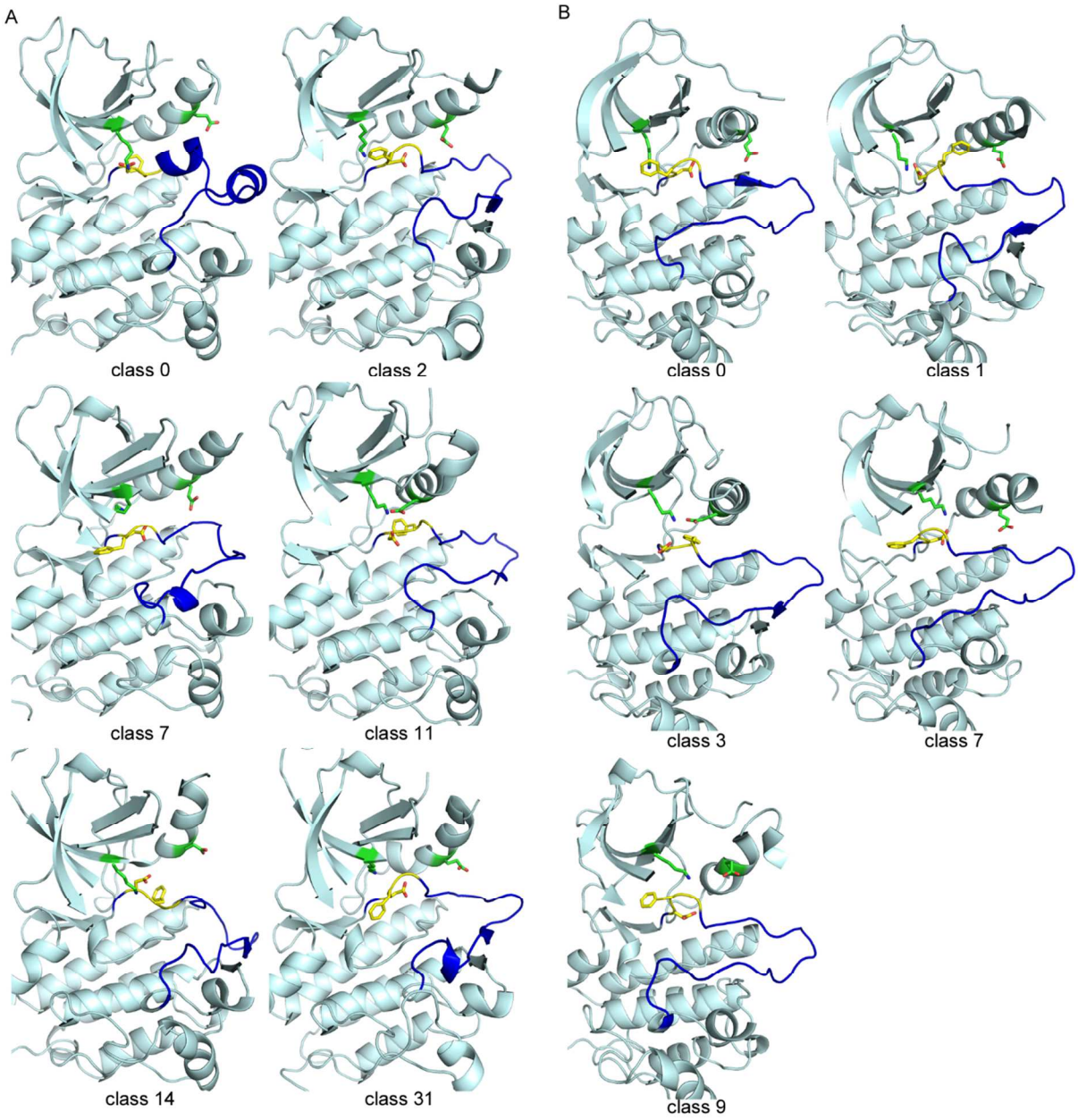

Figure S3. Representative structures of some classes from Bayesian clustering. A) Representative structures of six classes in ATI pathway. B) Representative structures of five classes in AI pathway. Structures in each class are described by the four metrics mentioned in main text. The structure closest to the centroid is selected as the representative structure of this class. The activation loop (A-loop) is colored blue; carbon atoms of the DFG motif are colored yellow; carbon atoms of Lys745 and Glu762 are colored green.

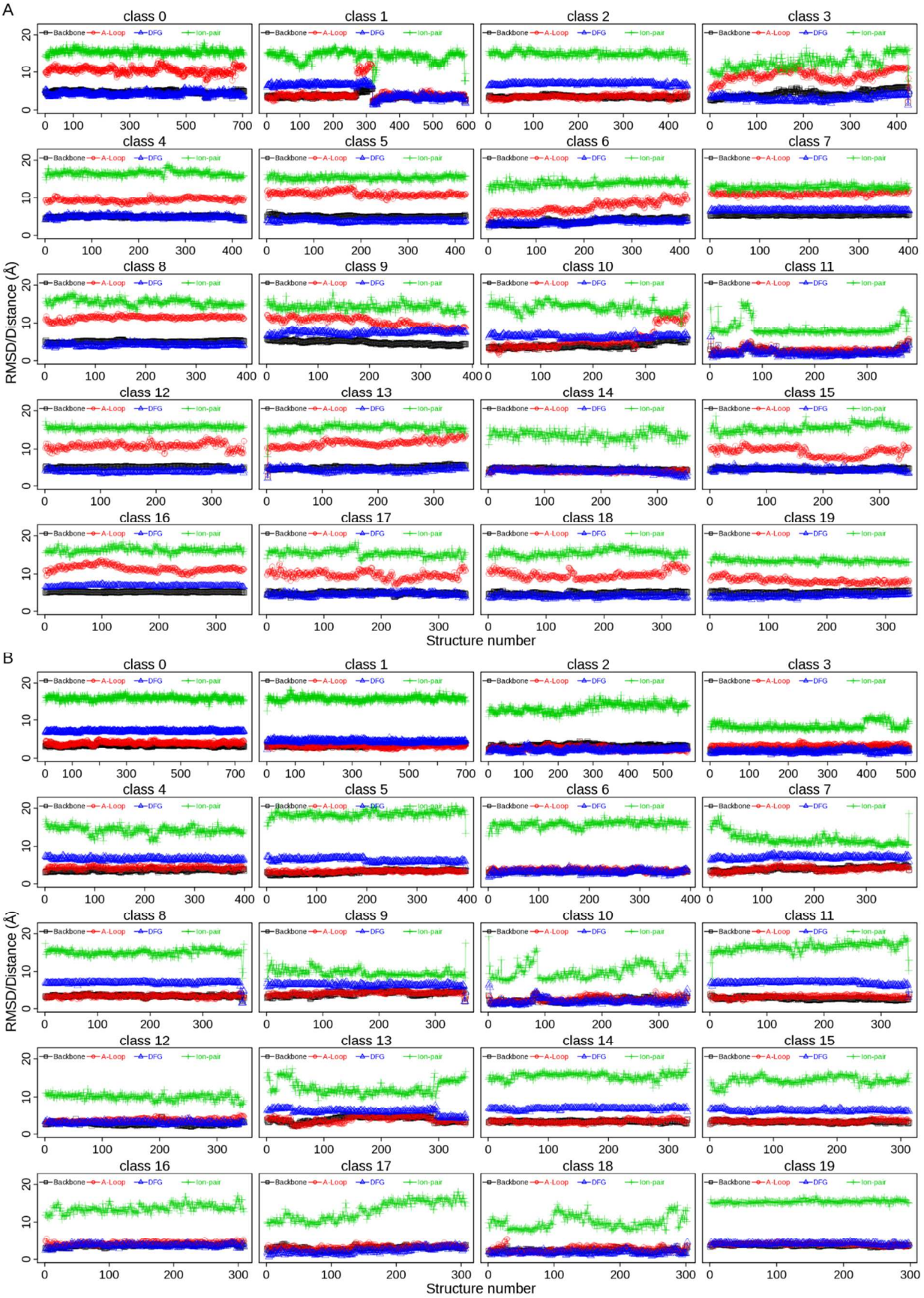

Figure S4. Evolution of structural properties in the top 20 populated classes from Bayesian clustering. A) Data from ATI pathway. B) Data from AI pathway. Four metrics are displayed: backbone RMSD, A-loop RMSD,

DFG RMSD and distance of ion pair (Lys-Glu). The RMSD values are calculated with respect to the crystal structure of 2ITW (form A).

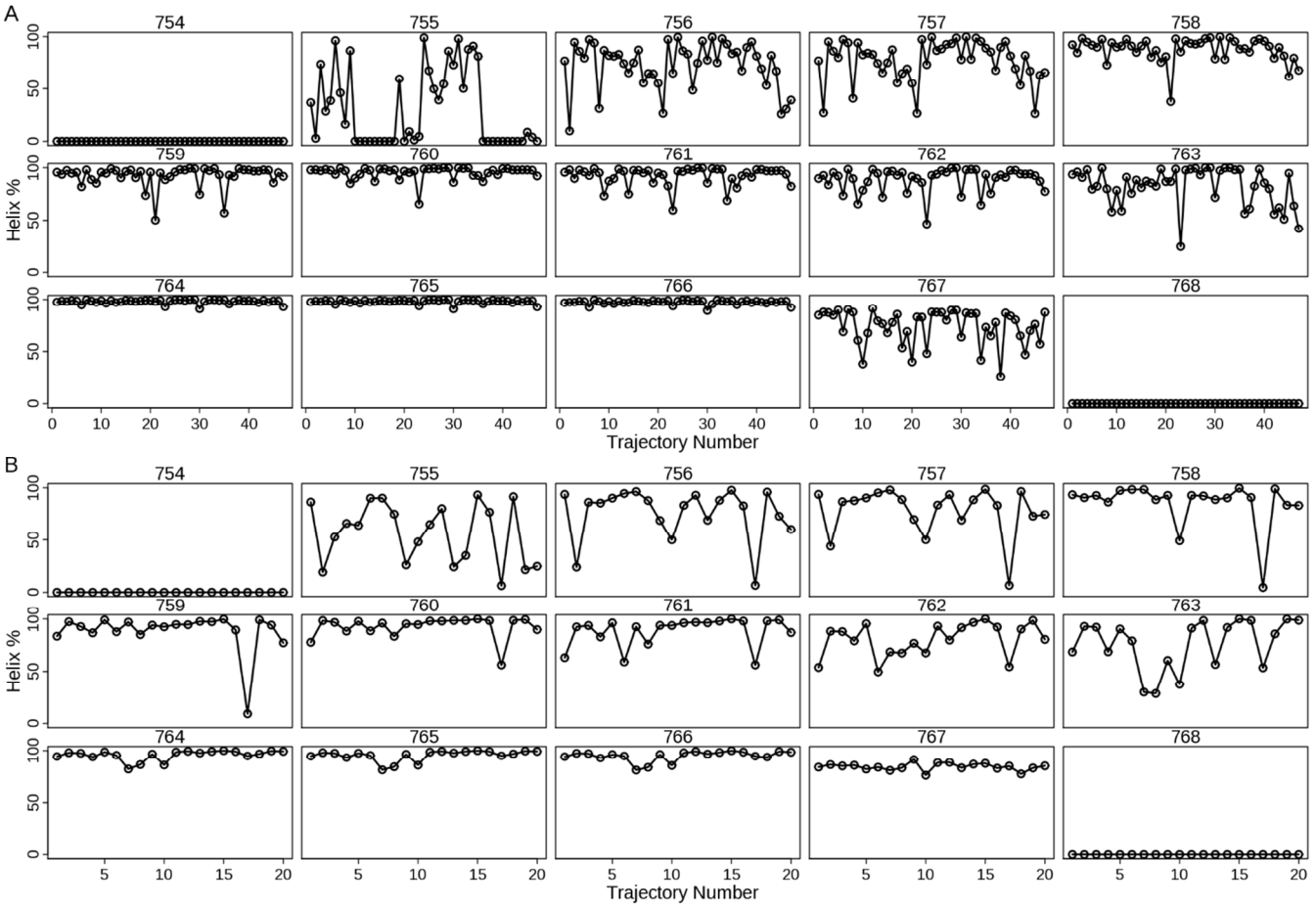

Figure S5. Percentage of alphaC helix (residues 754 – 768) in helix status in MD simulations. A) Data from 47 trajectories in ATI pathway. B) Data from 20 trajectories in AI pathway. The secondary structure information for each residue is calculated by ptraj implemented in Amber 11.

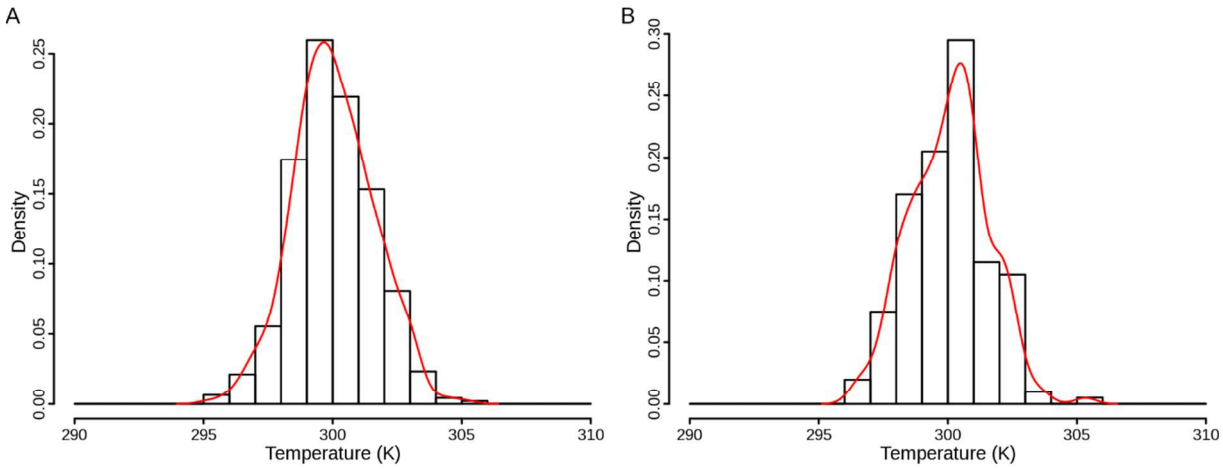

Figure S6. Distribution of temperatures in unbiased MD simulations. A) Temperature distribution from 47 MD trajectories in ATI pathway. B) Temperature distribution from 20 MD trajectories in AI pathway. 100 temperature values are extracted from each MD trajectory. The density is computed by the histogram analysis implemented in R v3.0. The bin width is 1 K.

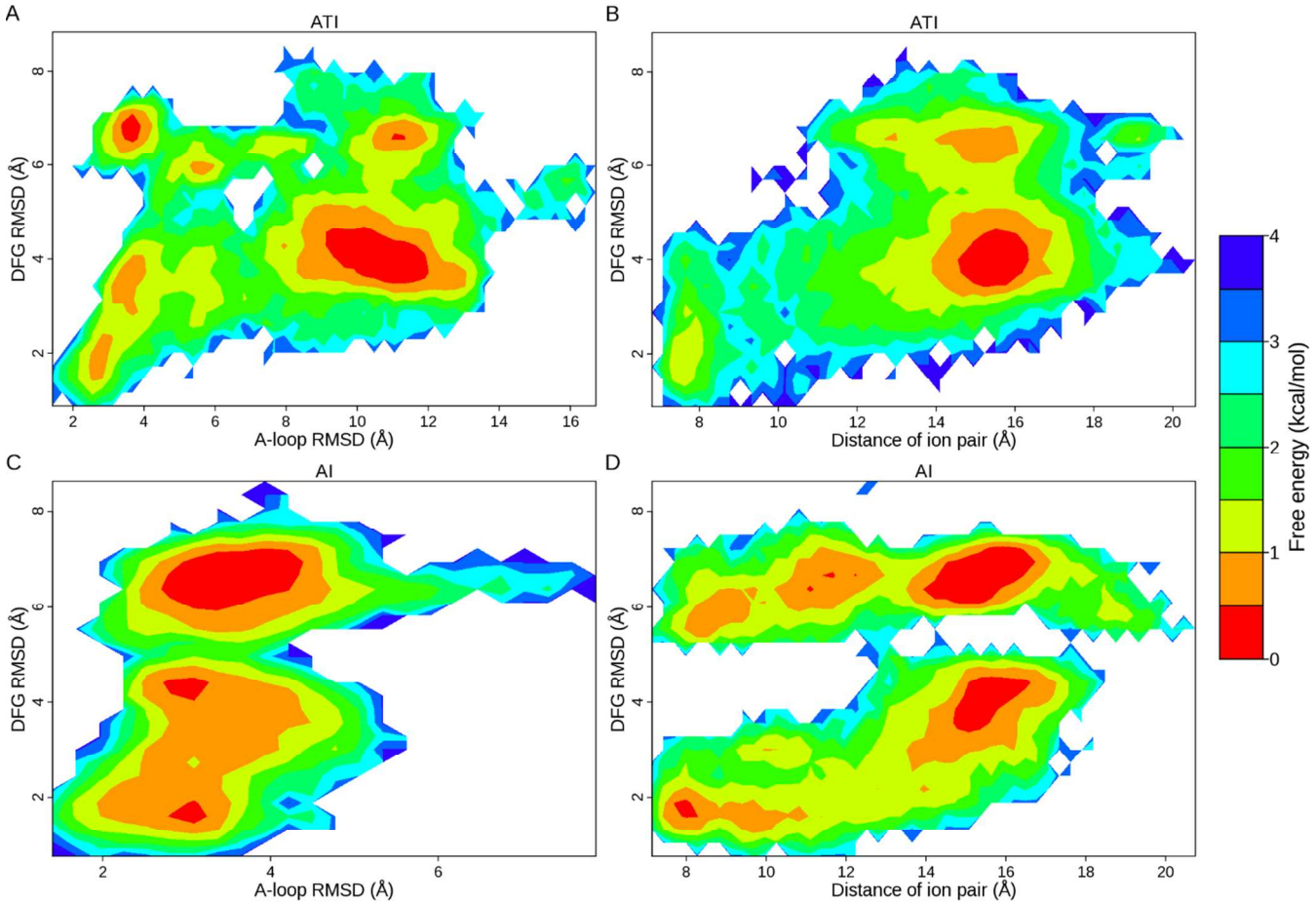

Figure S7. 2D free energy surfaces (FES) from sampled structures for Bayesian clustering. The FESs are calculated with sampled structures for Bayesian clustering. For ATI pathway, 23500 structures are used; for AI pathway, 20000 structures are used. FESs for ATI pathway are shown in A and B; FESs for AI pathway are shown in C and D. Three metrics are employed for FES plotting: DFG RMSD, A-loop RMSD and distance of ion pair. The RMSD values are calculated with the crystal structure of 2ITW (form A) as the reference. The 2D FESs display the same features with those in Figure 4.

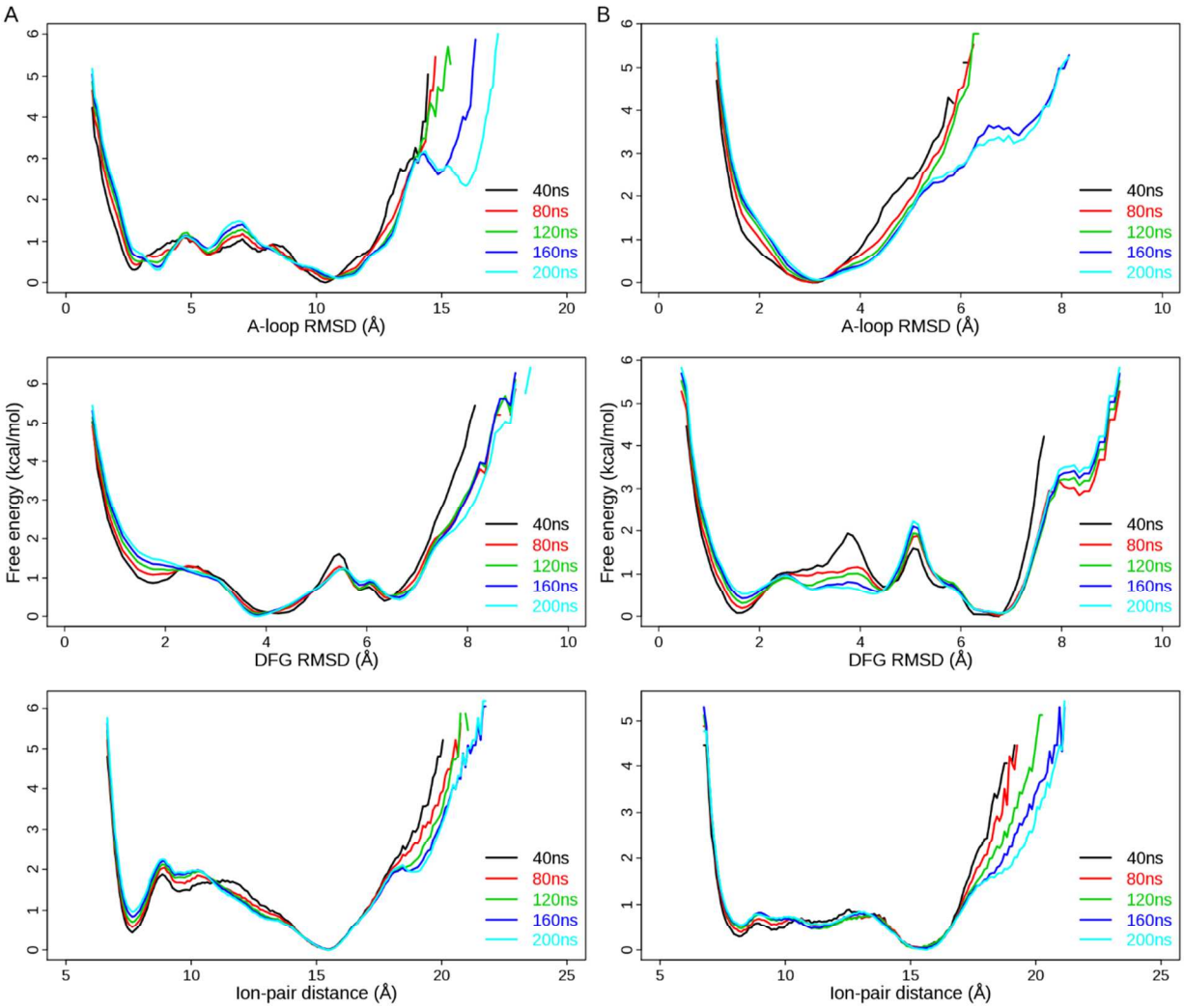

Figure S8. Convergence of free energy calculations. A) Data from 47 MD trajectories in ATI pathway. B) Data from 20 MD trajectories in AI pathway. One-dimensional free energy surface of EGFR kinase domain on three order parameters, A-loop RMSD, DFG RMSD and ion-pair distance, respectively, is calculated at an interval of 40 ns of simulation time.

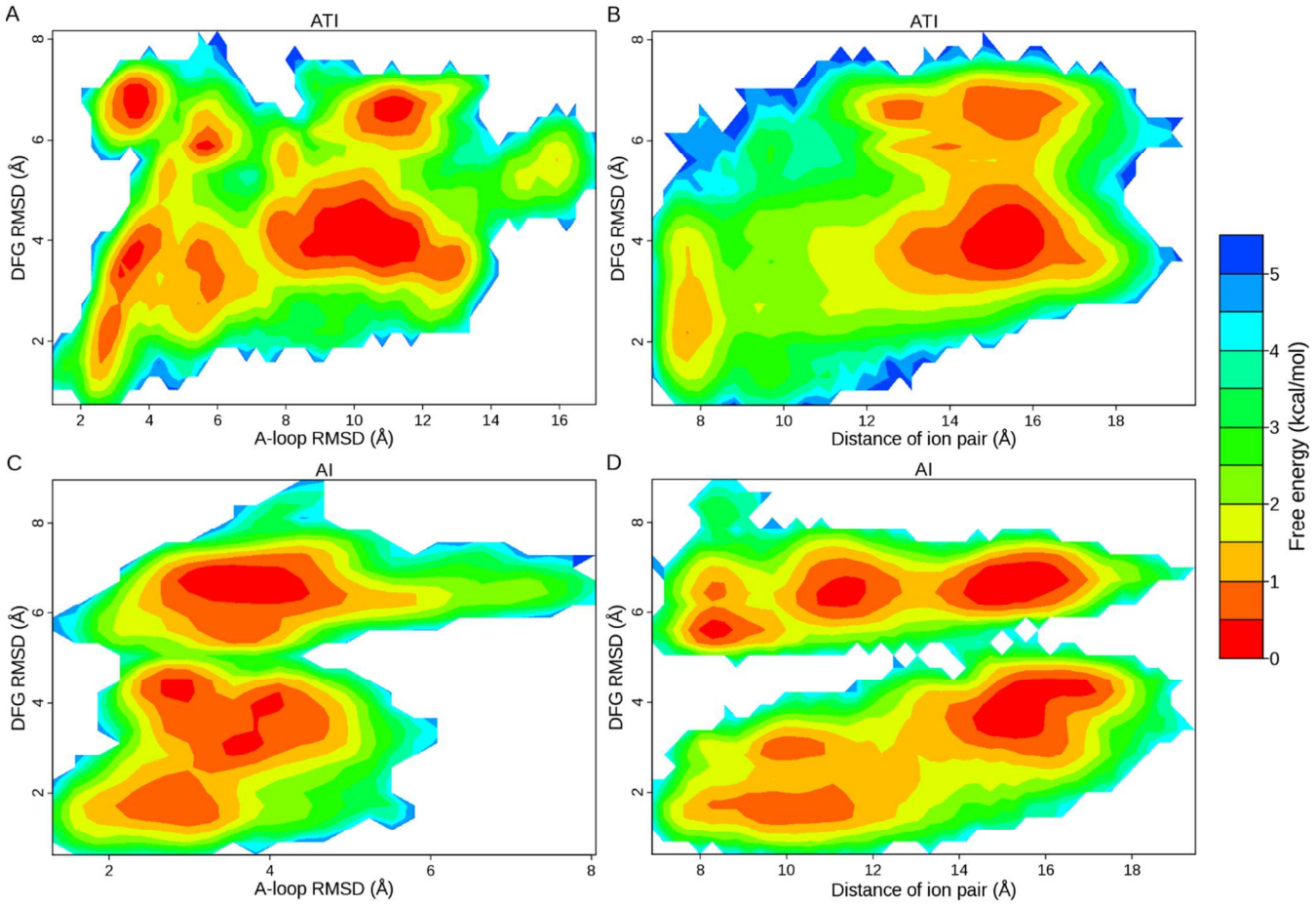

Figure S9. Influence of the number of seeding structures on 2D free energy surfaces. The snapshot structures obtained from K-means clustering are ranked by RMSD values. A subset of structures is obtained by selecting one structure every other one. Thus, for ATI pathway, there are 22 snapshot structures plus 3 crystal structures and totally 25 MD trajectories are employed for FES calculation. For AI pathway, 9 snapshot structures are chosen and totally 11 MD trajectories (plus 2 crystal structures) are employed for FES calculation. FESs for ATI pathway are shown in A and B; FESs for AI pathway are shown in C and D. Three metrics are employed for FES plotting: DFG RMSD, A-loop RMSD and distance of ion pair. The RMSD values are calculated with the crystal structure of 2ITW (form A) as the reference. Comparison with Figure 4 shows that transitions between some conformations are not sampled as well as those in Figure 4 though both figures display the same features.

Table S1. Average RMSDs in comparison with three EGFR crystal structures and ion-pair distance with standard deviation of top 20 populated classes from Bayesian clustering of 47 MD trajectories in ATI pathway.

Class No.	Backbone RMSD			A-loop RMSD			DFG RMSD			Distance of ion pair	Number of Structures
	A	I	T	A	I	T	A	I	T		
0	4.7±0.3	3.9±0.2	2.1±0.3	10.5±0.8	9.4±0.8	2.7±0.9	4.2±0.5	8.1±0.5	1.6±0.4	15.5±0.7	705
1	3.6±0.6	2.8±0.6	3.6±0.4	4.3±2.0	3.2±2.0	9.1±1.2	5.0±1.8	4.1±2.0	6.3±1.8	14.3±1.5	599
2	3.5±0.3	2.6±0.3	3.8±0.2	3.5±0.4	2.1±0.5	9.5±0.4	6.9±0.3	1.5±0.4	8.2±0.3	15.0±0.7	442
3	4.3±0.9	5.2±0.6	4.6±0.6	9.1±1.4	9.4±1.3	7.7±1.0	3.1±0.6	7.7±0.3	2.2±0.5	12.7±1.8	426
4	4.9±0.2	3.7±0.2	2.3±0.2	9.5±0.5	8.1±0.5	3.6±0.4	4.8±0.4	8.6±0.3	1.8±0.4	16.6±0.6	425
5	5.0±0.2	4.2±0.2	2.3±0.3	11.1±0.6	10.0±0.6	3.1±0.6	3.8±0.3	7.7±0.4	1.2±0.3	15.4±0.5	422
6	3.7±0.7	3.8±0.3	3.4±0.5	7.5±1.5	7.2±1.1	6.9±1.3	3.4±0.4	7.3±0.3	1.9±0.4	13.9±0.7	416
7	5.4±0.1	4.1±0.2	3.0±0.2	11.2±0.4	9.8±0.5	6.6±0.3	6.6±0.2	3.0±0.2	7.7±0.2	12.9±0.5	401
8	4.9±0.2	4.0±0.1	2.1±0.2	11.4±0.5	10.4±0.5	4.1±0.8	4.1±0.3	8.0±0.3	1.6±0.2	15.5±0.9	395
9	4.8±0.5	4.4±0.3	3.4±0.2	10.3±1.2	8.9±1.3	6.8±0.4	7.4±0.5	4.0±0.5	9.0±0.4	14.3±0.9	387
10	3.9±0.7	2.8±0.6	3.3±0.3	5.6±2.6	4.5±2.5	8.5±1.2	6.3±0.4	2.5±0.6	7.5±0.5	14.1±1.2	380
11	2.4±0.6	3.3±0.4	4.3±0.3	2.8±0.6	3.3±0.5	10.5±0.6	1.9±0.7	6.5±0.5	3.6±0.6	8.5±1.9	380
12	5.0±0.2	4.0±0.2	2.0±0.2	10.8±0.8	9.7±0.7	2.8±0.5	3.9±0.3	7.9±0.3	1.6±0.2	15.6±0.4	358
13	4.9±0.4	4.2±0.4	2.5±0.4	11.5±1.0	10.8±1.0	4.9±1.1	4.3±0.4	8.2±0.4	1.4±0.5	15.4±0.7	357
14	4.4±0.3	3.3±0.2	4.0±0.2	4.0±0.3	4.4±0.3	9.9±0.3	3.9±0.5	7.5±0.4	3.9±0.4	13.6±1.1	353
15	4.5±0.2	3.6±0.3	2.1±0.4	9.2±1.2	8.2±1.2	3.2±1.2	4.4±0.4	8.3±0.4	1.6±0.4	15.5±1.0	352
16	5.1±0.1	4.2±0.2	2.7±0.2	11.4±0.8	10.0±0.8	5.1±0.4	6.7±0.2	3.9±0.5	7.2±0.3	16.2±0.6	349
17	4.7±0.3	3.8±0.2	2.2±0.3	9.7±0.9	8.8±0.9	3.2±0.8	4.4±0.4	8.4±0.4	1.6±0.4	15.4±0.8	347
18	4.7±0.3	3.8±0.2	2.3±0.3	9.8±1.0	8.8±0.9	3.1±0.8	3.9±0.3	7.6±0.3	1.4±0.3	15.5±0.8	344
19	4.9±	4.2±	3.7±	8.2±0	7.5±0	6.1±0	4.0±	6.8±	3.1±	13.4±0.5	340

	0.3	0.4	0.3	.6	.8	.5	0.4	0.3	0.4		

Table S2. Average RMSDs in comparison with two EGFR crystal structures and ion-pair distance with standard deviation of top 20 populated classes from Bayesian clustering of 20 MD trajectories in AI pathway.

Class No.	Backbone RMSD		A-loop RMSD		DFG RMSD		Distance of ion pair	Number of structures
	A	I	A	I	A	I		
0	3.3±0.2	2.6±0.2	3.9±0.4	2.2±0.2	7.0±0.2	1.5±0.2	16.0±0.5	733
1	3.4±0.4	2.6±0.2	3.2±0.4	2.4±0.4	4.4±0.3	6.1±0.2	15.9±0.6	699
2	3.2±0.3	3.3±0.4	2.5±0.4	2.9±0.5	2.1±0.4	6.4±0.3	13.5±1.1	570
3	2.3±0.3	3.7±0.4	3.3±0.3	3.7±0.4	1.8±0.4	6.3±0.2	8.4±0.9	508
4	3.5±0.2	3.0±0.2	4.2±0.4	4.6±0.5	6.5±0.3	2.4±0.4	14.3±1.0	399
5	3.1±0.4	3.2±0.2	3.3±0.2	3.4±0.3	6.2±0.5	5.6±0.7	18.4±0.8	397
6	3.3±0.2	2.8±0.3	3.6±0.4	2.7±0.3	3.1±0.4	6.0±0.2	15.8±0.8	394
7	3.9±0.5	3.3±0.4	3.9±0.6	2.3±0.4	6.9±0.4	2.5±0.4	11.9±1.6	382
8	3.3±0.2	2.4±0.2	3.3±0.3	1.9±0.4	6.7±0.6	1.5±0.8	15.0±0.8	378
9	4.0±0.6	3.7±0.4	4.1±0.4	3.2±0.3	6.2±0.5	2.2±0.5	9.7±1.0	354
10	2.3±0.5	3.6±0.6	2.5±0.6	3.3±0.6	1.9±0.7	6.4±0.4	9.8±2.0	350
11	2.7±0.3	2.9±0.4	3.1±0.3	3.1±0.4	6.8±0.5	3.4±0.8	16.5±1.2	349
12	2.8±0.4	4.6±0.6	3.7±0.4	4.4±0.3	3.0±0.3	7.6±0.3	10.0±0.8	347
13	3.9±0.7	3.5±0.7	3.8±0.8	2.8±0.6	6.0±0.7	3.0±1.4	12.4±1.7	347
14	3.3±0.2	2.5±0.2	3.4±0.4	2.0±0.6	6.8±0.3	1.5±0.6	15.5±0.8	331
15	3.2±0.2	2.4±0.2	3.4±0.3	2.3±0.3	6.3±0.3	2.4±0.5	14.4±1.0	313
16	3.6±0.3	3.3±0.3	4.3±0.4	5.1±0.5	3.6±0.4	6.8±0.3	13.7±1.0	309
17	2.9±0.5	3.7±0.8	3.2±0.5	3.5±0.8	2.2±0.7	6.5±0.4	13.0±2.5	307
18	2.3±0.	3.7±0.	2.7±0.	3.6±0.	1.8±0.	6.6±0.	9.9±1.7	302

	3	6	6	7	4	3		
19	3.7±0.2	2.6±0.2	4.0±0.3	2.2±0.2	4.1±0.3	6.4±0.2	15.4±0.4	298